RSC Advances

PAPER

View Article Online
View Journal | View Issue

Cite this: *RSC Adv.*, 2025, **15**, 44373

Crystal violet removal from aqueous solution: adsorption studies, Box–Behnken optimization, safety, and reuse in methanol oxidation

Samar M. Mahgoub,[a] Abdullah S. Alawam,[b] Ahmed A. Allam,[b] M. Ramadan Mahmoud,[c] Asmaa Elrafey,[d] Ahmed Hashem Abdelmohsen[e] and Rehab Mahmoud *[f]

Received 1st October 2025
Accepted 2nd November 2025

DOI: 10.1039/d5ra07463k

rsc.li/rsc-advances

The discharge of toxic crystal violet (CV) dye poses significant environmental and health risks, necessitating sustainable treatment solutions. This study presents sulfuric acid-functionalized activated carbon derived from frankincense (SAC) as a high-performance adsorbent for CV removal. Characterization revealed a mesoporous structure with a high surface area of 842.97 $m^2\ g^{-1}$, adorned with functional groups that facilitate CV binding. Process optimization *via* Box–Behnken design achieved an exceptional adsorption capacity of 638.51 mg g^{-1} at pH 8, with a 0.075 g dose and 60 min contact time, following the Langmuir–Freundlich isotherm model. A pivotal finding from *in vitro* cytotoxicity assessment (HepG2 cells) was the effective detoxification of CV, where the half-maximal cytotoxic concentration (CC_{50}) increased dramatically from 84.7 μg mL^{-1} (untreated CV) to >1000 μg mL^{-1} (SAC-treated solution). Embodying circular economy principles, the spent adsorbent was successfully repurposed as an electrocatalyst for methanol oxidation, yielding a current density of 22.40 mA cm^{-2}. The process demonstrated economic viability at a low manufacturing cost of \$0.06438 g^{-1} SAC and excelled in green chemistry metrics (Eco-Scale: 90/100). This work underscores the dual utility of SAC as a sustainable, safe, and reusable material for advanced wastewater treatment and energy conversion applications.

1 Introduction

Rapid industrialization and urbanization have significantly increased the discharge of hazardous pollutants into aquatic environments, prominently synthetic dyes, which pose severe environmental and health risks.[1,2] Among these dyes, crystal violet (CV), a triphenylmethane compound widely used in leather, textile, and paper manufacturing, is especially concerning due to its persistence, toxicity, and resistance to biodegradation.[3–5] Even at low concentrations, CV inhibits photosynthesis, induces oxidative stress, and causes toxicity to aquatic life, leading to biodiversity loss and ecosystem disruption.[4,5] Furthermore, chronic exposure to CV in humans can result in mutagenic, carcinogenic, and teratogenic effects through ingestion, inhalation, or dermal contact.[6–9] Hence, effective removal of CV from wastewater is critical for environmental protection and public health.

Several approaches have been employed to remove dyes, including chemical precipitation,[10] membrane filtration,[11] and advanced oxidation processes.[12] However, these methods can be limited by high costs, secondary pollution, or operational complexity. Adsorption using activated carbon (AC) has garnered attention as an efficient, economical, and environmentally friendly alternative.[13–15] The quest for sustainable adsorbents has shifted attention towards lignocellulosic biomass precursors. Frankincense (Boswellia spp.), a natural resin, represents a promising, abundant, and low-cost precursor for AC production.[16–20] We hypothesize that subjecting frankincense powder to a simple one-step calcination process, coupled with simultaneous functionalization using sulfuric acid, will yield a novel activated carbon (SAC) with a high surface area, developed porosity, and abundant surface functional groups. These characteristics are critical for enhancing its adsorption affinity and capacity for cationic dyes like CV.[21–26] Furthermore, many adsorption studies focus solely

[a]*Materials Science and Nanotechnology Department, Faculty of Postgraduate Studies for Advanced Sciences, Beni-Suef University, Egypt. E-mail: miramar15@yahoo.com*
[b]*Department of Biology, College of Science, Imam Mohammad Ibn Saud Islamic University (IMSIU), Riyadh 11623, Saudi Arabia. E-mail: asalawam@imamu.edu.sa; aallam@imamu.edu.sa*
[c]*Faculty of Pharmacy, Al-Azhar University, Assiut, Egypt. E-mail: www.mohamedramadan@gmail.com*
[d]*Environmental Science and Industrial Development Department, Faculty of Postgraduate Studies for Advanced Sciences, Beni-Suef University, Beni-Suef, Egypt. E-mail: asmaa_elrafey@hotmail.com*
[e]*The Central Laboratory, Faculty of Postgraduate Studies for Advanced Science (PSAS), Beni-Suef University, Beni-Suef 62511, Egypt. E-mail: Ahmed.h.abdelmohsen@gmail.com*
[f]*Department of Chemistry, Faculty of Science, Beni-suef University, Beni-suef 62528, Egypt. E-mail: rehabkhaled@science.bsu.edu.eg*

on removal efficiency, often neglecting the subsequent biological safety of the treated effluent and the fate of the spent adsorbent, which can pose a secondary waste problem. We propose that the SAC we synthesize will not only effectively remove CV but also significantly detoxify the solution, a hypothesis we will test using *in vitro* cytotoxicity assays. Moreover, embracing a circular economy model, we hypothesize that the spent CV-laden adsorbent (SAC/CV) can be repurposed as a valuable resource rather than discarded. Specifically, we will investigate its potential application as an electrocatalyst for the methanol oxidation reaction (MOR), adding a valuable second life to the material and enhancing the overall sustainability of the process.[27–30]

Therefore, the present study is systematically designed to: (i) synthesize and comprehensively characterize sulfuric acid-functionalized activated carbon from frankincense powder (SAC); (ii) evaluate its performance in the adsorption of CV dye from aqueous solutions, optimizing key parameters such as pH, adsorbent dose, contact time, and initial concentration using Response Surface Methodology (RSM); (iii) analyze the adsorption kinetics, isotherms, and thermodynamics to elucidate the underlying mechanism; (iv) assess the biological safety of the SAC-treated water using HepG2 cell lines to confirm detoxification; and (v) explore the innovative valorization of the spent adsorbent by evaluating its electrocatalytic performance in methanol oxidation. This integrated approach aims to present SAC as a sustainable, high-performance, and multifunctional material that advances environmental remediation while contributing to energy-related applications. Table 1 summarizes recent adsorbents for CV removal, contextualizing the superior performance of SAC within current literature.

2 Materials and methods

2.1 Chemicals and reagents

Frankincense was purchased from Kush Aroma Exports in Kannauj, India. Merck (Darmstadt, Germany) furnished crystal violet, 37% hydrochloric acid, acid (H_2SO_4), base (NaOH), and distilled water. The samples were analysed using a Thermo Fisher Scientific Evolution 350 UV-Vis Spectrophotometer. The American Type Culture Collection (Manassas, VA, USA) provided HepG2 human hepatocellular carcinoma cells (ATCC® HB-8065™) for biological safety testing. Sigma-Aldrich supplied Dulbecco's Modified Eagle Medium (DMEM), fetal bovine serum (FBS), penicillin-streptomycin solution, and 3-(4,5-dimethylthiazol-2-yl)-2,5-diphenyltetrazolium bromide (MTT) reagent. Gibco provided phosphate-buffered saline (PBS) and a trypsin-EDTA solution.

2.2 Preparation of sulfuric acid-functionalized activated carbon derived from frankincense powder

Two grams of frankincense powder was first mixed with 1 mL of concentrated sulfuric acid. The mixture was then calcined in a muffle furnace at a high temperature of 800 °C for a fixed period of 30 minutes. After calcination, the resulting material was washed repeatedly with distilled water until the pH reached nearly 7 to remove residual acid and impurities. After washing, the sample is typically filtered or centrifuged to separate the solids before drying. The washed SAC was dried at 100 °C. The resulting SAC is ground to a finer consistency for better uniformity and performance. To achieve reproducibility, we used consistent amounts of frankincense and acid, fixed the experimental conditions such as temperature/time for calcination, and washed the samples to confirm the reproducibility of the SAC batches (Fig. 1). In addition to batch preparation, monitoring key factors such as the temperature homogeneity of the material used with the acid inside the furnace is essential. Every batch of characterization data was compared across batches to assess variation.[37–39]

2.3 Material characterization

The adsorbent material was characterized using a PANalytical X-ray diffractometer (Empyrean, Almelo, The Netherlands) with Cu-Kα radiation (wavelength of 0.154 nm, I = 35 mA, scanning rate of 8° min^{-1}, V = 40 kV). The crystallinity and structure were determined by scanning from 5° to 80° (2θ) at 8° min^{-1}. The functional groups were analysed using FTIR spectroscopy with a Bruker Vertex 70 spectrometer using the KBr pellet procedure (Berlin, Germany). To detect chemical bonding on the sample surface, measurements were taken between 400 and 4000 cm^{-1}. The SCVs' morphology was examined using field-emission scanning electron microscopy (FESEM) on a ZEISS Sigma 500 VP system (Jena, Germany). This high-resolution microscope obtains full views of surface patterns and topography, producing in clear, high-contrast images suitable for analyzing the SCV's microstructure. The CV concentrations were determined with a SHIMADZU UV-2600 UV-VIS spectrophotometer

Table 1 Adsorbents for CV removal reported in earlier open literature studies

Adsorbent	pH	Adsorbent mass ($g\ L^{-1}$)	Equilibrium time	q_{max} ($mg\ g^{-1}$) for CV	Reference
SAC	8.00	0.075	60 min	638.51	This work
Bentonite-alginate composite	8.00	0.50	—	601.93	31
Sodium dodecyl sulfate (SDS)	8.00	0.20	60 min	—	32
Charred rice husk (CRH)	10.00	0.025	60 min	62.85	33
Xanthate rice husk (XRH)	10.00	0.025		90.02	34
TLAC/Chitosan composite	9.00	0.40	40 min	500	35
Fr-fMWCNT-Fe_3O_4	6	0.05	25 min	500	36
Fr-fMWCNT	6	0.04	30 min	439	36

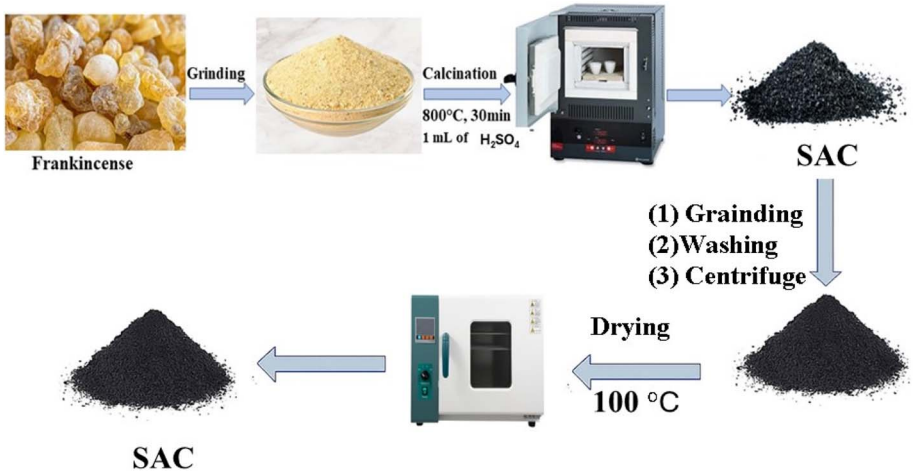

Fig. 1 Schematic representation of the process for preparing activated carbon from frankincense.

(Kyoto City, Japan). The pH of the solution was measured with an automatic surface pH meter (Adwa-AD1030, Szeged, Hungary). Nitrogen adsorption–desorption isotherms were calculated using a TriStar 3020 system (Micromeritics, Norcross, GA, USA), including the Brunauer–Emmett–Teller surface area, pore volume, and pore diameter.

2.4 Adsorption study

Adsorption studies were performed using equipment specifically developed for a series of room temperature trials. A 1000 mg L^{-1} CV standard solution was used to generate a calibration curve spanning values ranging from 5 to 500 mg L^{-1}. The adsorption experiment consisted of pouring a 100 mg L^{-1} CV solution in 50 mL Falcon tubes and adding 0.05 g of SAC. A Metrohm 751 Titrino was used to measure the pH of the solutions after they had been adjusted to 3, 5, 7, 8, and 10 using 0.1 N NaOH or HCl. To achieve equilibrium, the tubes were shaken for 24 hours at 250 rpm using an orbital agitator (SO330-Pro). After this stage, filtration was done with a 0.22 μm Millipore nylon syringe filter.

A UV-visible spectrophotometer was used to measure the CV concentration at 587 nm before and after adsorption.[40] The following calculations were used to calculate the percentages of clearance and amount of CV adsorbed (Qe):

$$Q_e = \frac{(C_o - C_t)V}{W} \quad (1)$$

$$\text{Removal percent}(R) = \frac{C_o - C_t}{C_o} \times 100 \quad (2)$$

where W is the adsorbent's mass in grams (g), V is the CV solution's volume in liters (L), Q_e is the amount of CV adsorbed per gram (mg g^{-1}), C_o is the initial CV concentration (mg L^{-1}), and C_t is the CV concentration after adsorption at time t (mg L^{-1}). A constant CV concentration of 100 mg L^{-1} was utilised to evaluate various amounts of SAC (range from 0.05 g to 0.20 g) to investigate the effect of adsorbent dose. The final pH of each solution was measured after the adsorption process.

Furthermore, using a constant adsorbent mass of 0.075 g and an optimal pH of 8, the effects of various CV concentrations (ranging from 5 mg L^{-1} to 500 mg L^{-1}) were examined. Adsorption data were analysed with two-, three-, and four-parameter isotherm models. Finally, four different temperatures (25 °C, 35 °C, 45 °C, and 55 °C) were used to evaluate the effect of temperature on adsorption and calculate thermodynamic parameters. Pseudo-first-order (PFO) is one of the models used to explore the adsorption kinetics of CV on synthetically activated carbon. Pseudo-second-order (PSO),[41] intraparticle diffusion[42] and Avrami[43] at various time points from 0–240 minutes. These models were evaluated at different intervals ranging from 0 to 240 minutes. The best-fit model for adsorption was determined by error function analysis.[44] The effects of water type on SAC treatment of CV dye-contaminated raw water samples were investigated. Four different types of water were tested: distilled water (D.W.), tap water (T.W.), raw groundwater (G.W.), and secondary treated wastewater (effluent from a municipal treatment plant after biological processes, which typically removes organic matter but may contain dissolved ions and nutrients). In each experiment, 0.07 g of SAC was combined with 100 mL of water containing 5 ppm CV and stirred at pH 8 for 2 hours. We utilised a UV-Vis spectrophotometer to measure residual CV concentrations.

2.5 Working electrode preparation and electrochemical methanol oxidation using the spent SAC

Following adsorption, the unused SAC powder was collected, washed, and dried at 80 °C for 24 hours. A graphite sheet electrode (GS) proved to be the most effective working electrode modification for methanol oxidation. A slurry of 5 mg of waste SAC88 in 400 μL of isopropanol and 15 μL of 5% Nafion solution was sonicated for 30 minutes at room temperature. The GS electrodes received 10 μL of the sonicated solution. The electrode surface was then dried for another 30 minutes at 60 °C.

The electrocatalytic activity of SAC and SAC/CV was measured using a potentiostat/galvanostat (AUTOLAB PGSTAT

302 N, Metrohm, Herisau, Switzerland) and NOVA 1.11 software. A standard three-compartment glass cell was employed at room temperature, with a Pt wire counter electrode, a GS, and an Ag/AgCl reference electrode. The electrocatalytic activity of the produced electrodes was tested using a 1 M NaOH electrolyte solution with and without methanol. The cyclic voltammetry experiments were conducted at scanning rates ranging from 10 mV s^{-1} to 100 mV s^{-1} in the potential range of 0 to 0.90 V. CA measurements took 3600 seconds at 0.6 V.

2.6 Box–Behnken design

The Box–Behnken design (BBD) methodology is a methodical and successful approach to experimental design, ensuring a comprehensive understanding of the expected response.[45–47] This method emphasizes the importance of important independent parameters, such as pH, contact time, initial concentration, and adsorbent dosage, in maximizing the anticipated reaction.[48] This study includes adsorption experiments created inside the BBD framework, using the extensive statistical capabilities of Design Expert (Stat-Ease, Version 13).[48,49] Table 2 displays a dataset containing the factor levels under consideration, as well as their associated coded values. The basic idea behind this method is to employ a second-degree polynomial model, as shown in eqn (3), to accurately reflect the relationship between independent elements and the dependent response.

$$Y(\%\ \text{of CV reduction}) = \beta_O + \sum_{i}^{k} \beta_i X_i + \sum_{ii}^{k} \beta_{ii} X_i^2 + \sum_{ij}^{k} \beta_{ij} X_i X_j \quad (3)$$

In this scenario, X_i and X_j indicate the variables being researched, while Y represents the expected result, which in this case is the CV domain. The observed elimination process was the product of twenty-nine systematic designed trials. The foundation for the CV removal trials was built by accurately measuring a predetermined amount of activated carbon and properly mixing it with 100 mL of CV solution.

Response surface methodology (RSM) is a legitimate statistical technique for determining the greatest possible combination of various elements to yield the best possible experimental results. The Box–Behnken design (BBD) methodology differs from the other RSM methods. In four-factor fractional factorial designs, BBD uses exact mathematical models to find first- and second-order interactions.[46–50] This methodology is presented by a case study in which the adsorption efficiency is optimised in terms of pH, starting concentration, adsorbent dosage, and contact time. The experimental technique consists of three phases: zero, positive, and negative. RSM provides a rigorous framework for picking the best results, allowing scientists to optimize process efficiency and adjust the experimental circumstances.[49]

Table 2 Actual variables, corresponding codes, and their BBD levels

Independent variables	Code	Low level (−1)	Centre level (0)	High level (+1)
Initial concentration	A	5.00	252.50	500.00
Time of contact	B	10.00	245.00	480.00
Adsorbent dosage	C	0.05	0.13	0.200
pH	D	3.00	6.50	10.00

2.7 Assessment of the greenness profile of the method

Several aspects influence environmentally conscious analytical procedures, including the amount and toxicity of chemicals used, waste generation, energy consumption, the number of procedural stages, as well as their degree of automation and minimization. To comprehensively evaluate the sustainability and greenness profile of our proposed strategy, multiple assessment methodologies were employed, including the National Environmental Methods Index (NEMI), Analytical Greenness Profile (AGP), and the modified Green Analytical Procedure Index (Mo GAPI). The Analytical Greenness Calculator (AGREE) and the Analytical Eco-scale were also utilized to quantify greenness. The Eco-scale score, the first technique presented, assigns penalty points based on factors such as power consumption, waste, reagents, and toxicity. After accounting for these, the total penalty points, subtracted from a perfect score of 100, provide a quantitative measure of the method's greenness. AGREE further complements these by providing a comprehensive, flexible, and straightforward assessment based on the 12 principles of green analytical chemistry, yielding an easily interpretable pictogram that visualizes the overall greenness score and the performance in each criterion.[51,52]

The newly designed Blue Applicability Grade Index (BAGI) tool was applied to evaluate the analytical technique's "blueness," utility, and application. This "blueness" represents a composite metric reflecting the practicality and usability of an analytical method. BAGI calculates this metric by scoring ten key operational attributes, including the type of assessment, the total number of analytes, instrumentation requirements, sample effectiveness, requirements for sample preparation, analysis throughput, consumption of reagents and materials, degree of automation, sample volume, and the concentration range of analytes. The result is both a numerical score and a color-coded visual "asteroid" pictogram, which makes the evaluation of method practicality intuitive and facilitates comparison across analytical techniques. This tool thus adds a valuable dimension to the greenness profile by embracing method applicability and operational feasibility alongside traditional environmental parameters.[53,54]

3 Results and discussion

3.1 Characterization of tested materials

3.1.1 Fourier transform infrared (FT-IR) of the tested materials. Fig. 2a shows the FT-IR spectrum of the sulfuric acid-functionalized activated carbon derived from the frankincense powder. This explanation involves analyzing the functional groups and their corresponding peaks in the spectrum before the adsorption of crystal violet. SAC contains a porous structure

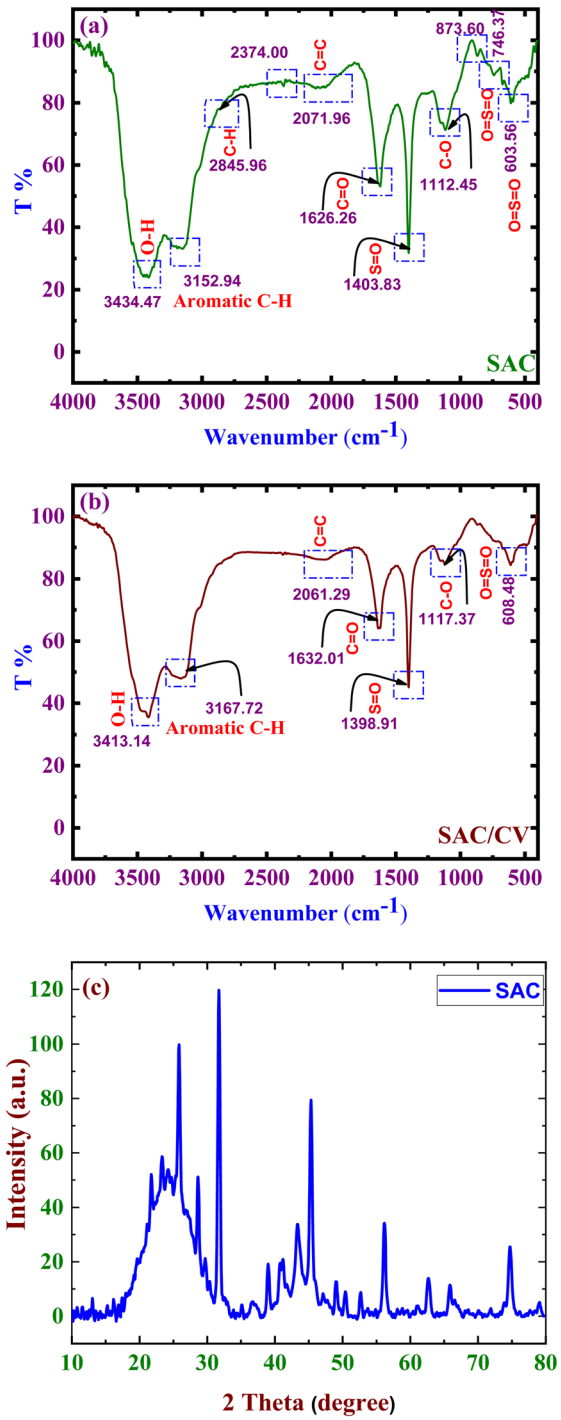

Fig. 2 FTIR spectra (a) before; (b) after CV dye and (c) XRD pattern of the SAC and removal on the SAC.

with surface functional groups, including hydroxyl and carbonyl groups. The functionalization with sulfuric acid is expected to introduce sulfonic acid (–SO_3H) groups and may modify existing functional groups.[55] Moreover, we expect the transformation of all frankincense powder precursors into activated carbon, but this precursor contains natural organic compounds, such as terpenoids, which may influence the FTIR spectrum. Common functional groups in activated carbon, such as O–H stretching, produce broad peaks at approximately 3200–3600 cm^{-1}, C–H stretching produces peaks at approximately 2800–3000 cm^{-1} (sp^3 and sp^2 hybridized carbons), which indicate residual aliphatic hydrocarbons, C=O stretching produces a strong peak at approximately 1650–1750 cm^{-1}, C=C stretching produces peaks at approximately 1500–1600 cm^{-1}, and C–O stretching produces peaks at approximately 1000–1300 cm^{-1}. Owing to functionalization with sulfuric acid, specific peaks appear due to –SO_3H groups, such as S=O stretching, which produces peaks at approximately 1100–1200 cm^{-1}, and O=S=O symmetric/asymmetric stretching, which produces peaks at approximately 1000–1400 cm^{-1}. Interestingly, the changes in the O–H and C=O regions indicate interactions with sulfuric acid. In addition, the reduction in the intensity or disappearance of peaks at approximately 1650–1750 cm^{-1} is expected due to the consumption of carbonyl groups during the functionalization process. The peaks at approximately 1500–1600 cm^{-1} indicate aromatic ring structures, which remain intact or slightly shift. In summary, the FTIR spectrum of the SAC powder shows characteristic peaks of sulfonic acid groups at 1000–1400 cm^{-1}, confirming successful functionalization. The broad O–H stretching bands at 3200–3600 cm^{-1} indicate the presence of hydroxyl groups, whereas changes in the C=O region suggest chemical modifications during the functionalization process. The presence of all of these functional groups is expected to recommend our materials for adsorption applications, as they improve adsorption capabilities.[53] Also, a strong signal associated with the asymmetric stretching of S=O appeared at around 1403.83 cm^{-1}. A broad transmission band at around 1112.45 cm^{-1} commonly existed in the spectra of the oxidized carbons and was attributed to stretching of the C–O group from alcohol, acids, phenols, ethers, and/or ester functional groups. As well as O=S=O bending vibrations may be observed at approximately 500–700 cm^{-1} (746.37 cm^{-1} and 603.56 cm^{-1}). In addition, there are broad peaks at approximately 3434.47 cm^{-1} due to stretching vibrations, which are often indicative of hydrogen bonding or moisture. Moreover, C=C stretching vibrations in aromatic rings appear near 1500–1600 cm^{-1}, and C–H stretching vibrations appear at approximately 2800–3000 cm^{-1} (Fig. 2a).

Additionally, Fig. 2b shows the FT-IR spectra of our materials (SAC) after removal of the CV dye. It is well known that CV dye is a cationic organic compound, so that during adsorption, the functional groups of the dye may interact with the carbon surface active sites. After dye removal, changes in these interactions are observed in the spectrum. Key functional groups will be identified with characteristic peaks such as a decrease in the sulfonic acid peak intensity or slight shifts, which may indicate interactions with the CV. In Fig. 1a, the infrared transmission peak that appeared at 1626.26 cm^{-1} was attributed to C=O stretching vibrations of the conjugated hydrocarbon.[56–58] We noted the appearance of dye-related peaks because the residual dye remained (Fig. 2b), including aromatic rings or tertiary amines.[59–61] With respect to aromatic rings, the characteristic peaks typically appear in the following regions: aromatic C–H at approximately 3167.72 cm^{-1}, aromatic C=C at approximately 1632.37 cm^{-1}, and C–H out of plane bending at approximately

675–900 cm^{-1}. C–N stretching (amine groups) appears at approximately 2081.29 cm^{-1}. Finally, the shifts in the hydroxyl peaks and changes in the broad OH peak and the disappearing of peaks appearing in 2845.96, 2374.00, 873.60 and 746.37 cm^{-1} might suggest interactions with the dye molecules.

The analysis of FTIR concerned with the intramolecular H-bonding among the SAC and CV molecules. The hydrogen bonding intensity was calculated from the ratio of the absorbance bands related to the –OH peak and the C=O peak in SAC and SAC/CV one wavenumber, respectively, showing

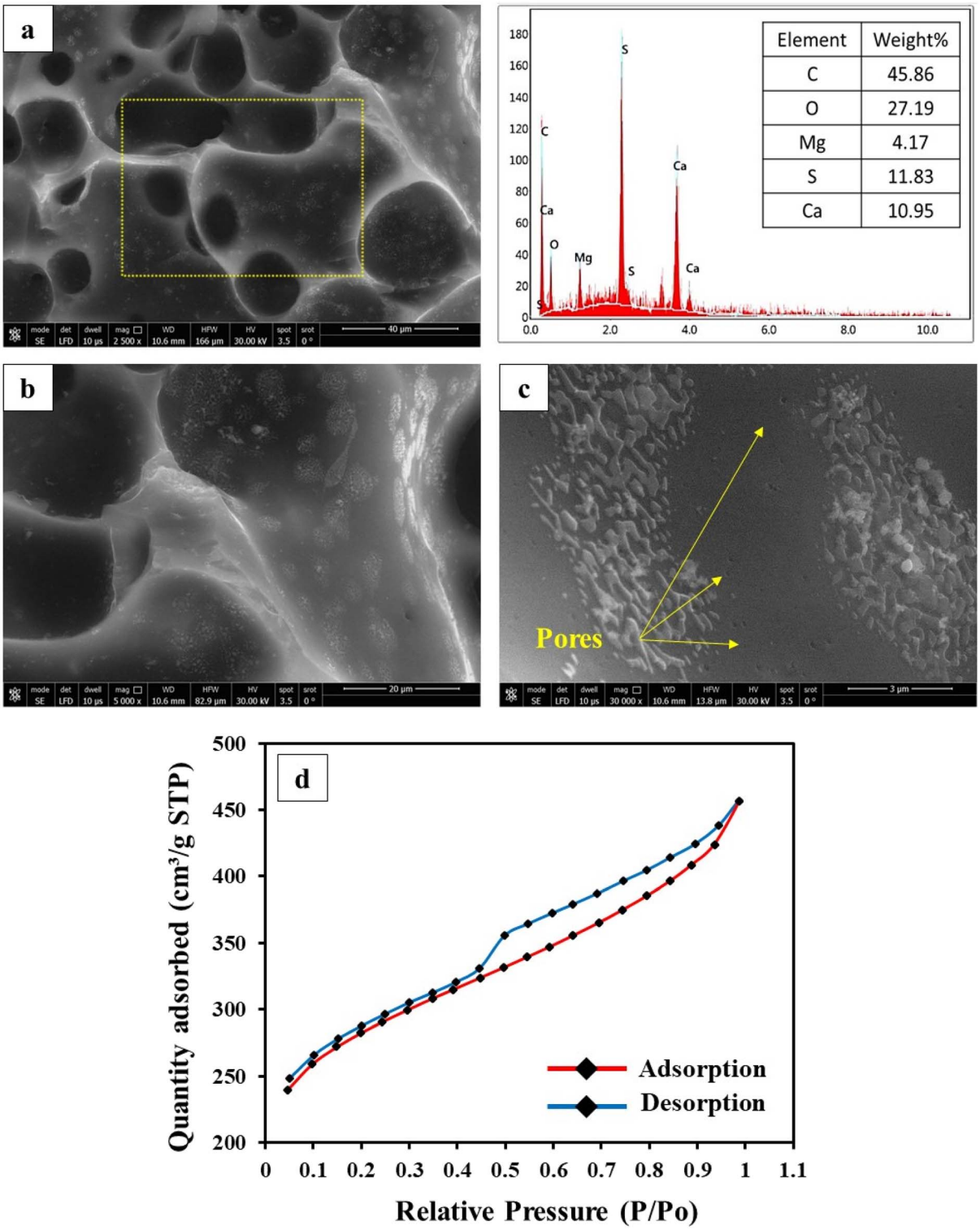

Fig. 3 (a–c) SEM-EDX and (d) BET analysis of the SAC.

a significant increase in the case of the after adsorption sample (0.55) compared to that before adsorption (0.44), confirming the H-bonding interactions between the CV molecules and SCV and successful adsorbing of CV onto the SAC surface[62] (Fig. 2b).

3.1.2 XRD analysis. Fig. 2c shows the crystalline structure and peaks of the SAC powder. The XRD pattern's large hump/peak between 20° and 30° (2θ) indicates amorphous/disordered carbon. This demonstrates the presence of activated carbon compounds. In contrast, strong peaks in the XRD pattern suggest the existence of crystalline phases. These peaks could be attributed to residual mineral content or inorganic contaminants in the original frankincense powder. Furthermore, this could be due to the injection or synthesis of crystalline sulfur compounds during the sulfuric acid functionalization process. The steep peak at approximately 26° (2θ) is commonly associated with the (002) reflection of graphitic carbon, indicating graphitic layers with some crystallinity. The sharp peaks at 40°, 50°, and 60° (2θ) may indicate the presence of sulfur-based compounds such as sulfates or other crystalline impurities.[59–63]

3.1.3 Morphology and surface studies (FESEM, EDX, and BET analysis). Figure 3a and b shows SEM (scanning electron microscopy) images of the SAC morphologies at various magnifications. The SAC showed folds with a rough surface and numerous pores, whereas a previous study revealed pictures of frankincense with a smooth, nonporous surface.[64] Porous particles have larger surface areas than nonporous particles do.[65] As a result, it was predicted that the SAC would result in a larger surface area. The BET results revealed that the increased surface area of the SAC impacted the rate of dissolution, which facilitated drug adsorption. Fig. 3c shows the EDX results for the material's elemental makeup as analyzed for the SAC.

Fig. 3d depicts the utilization of nitrogen adsorption/desorption isotherms to determine the SAC's porosity and surface area. BET surface area was measured as 842.965 $m^2\ g^{-1}$. The IUPAC classifies this isotherm as type IV, indicating a combination of microporous and mesoporous materials. Aggregates (loose assemblages) of plate-like particles produce slit-like pores and are linked to an H3 hysteretic loop. Its

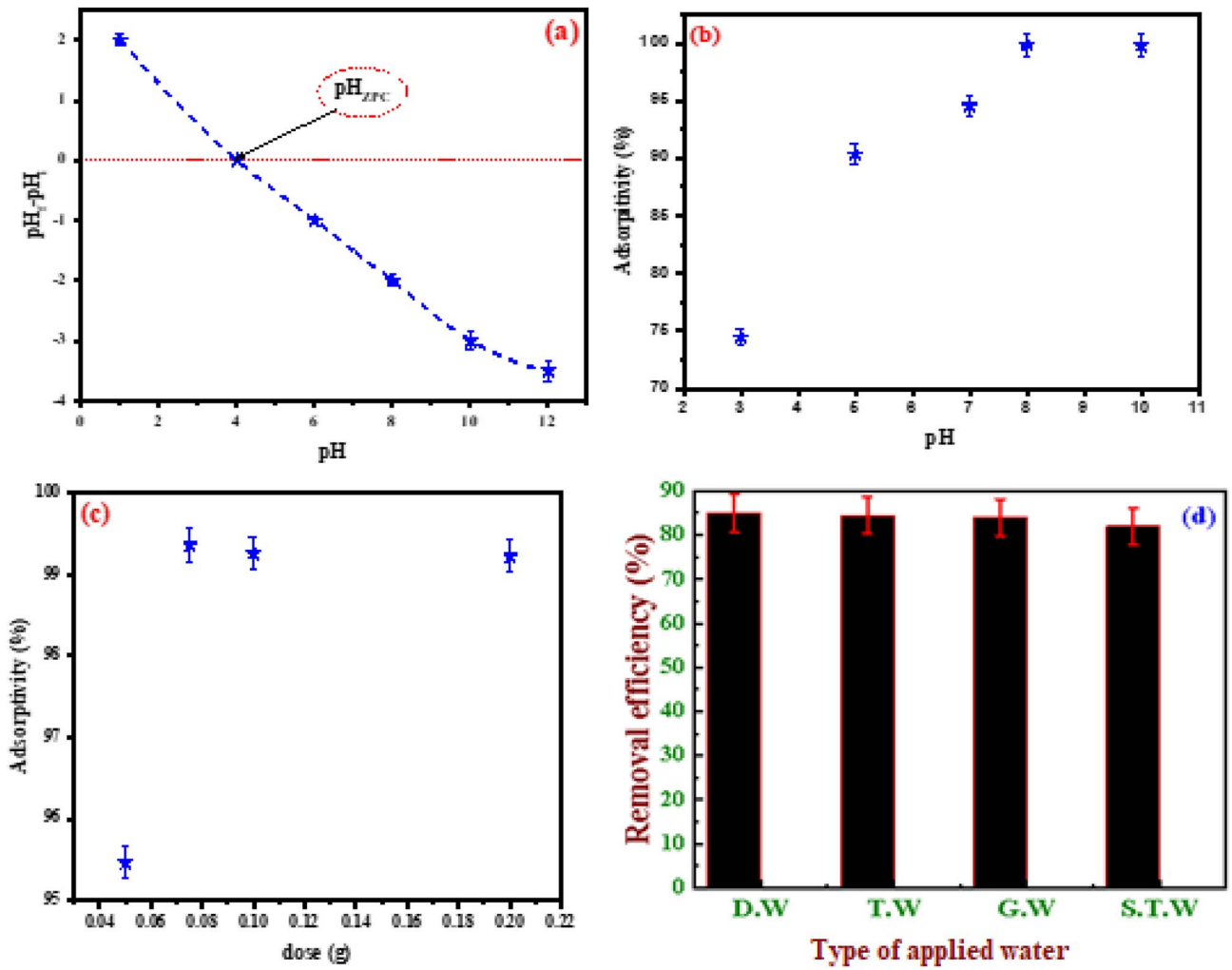

Fig. 4 (a) Point of zero charge (PZC) of the SAC; (b) Effect of solution pH on CV removal efficiency; (c) effect of adsorbent dosage on CV removal efficiency; and (d) effect of water matrix on CV removal efficiency.

mesoporous nature is confirmed by its pore size range of 2–50 nm, which is extremely favorable for boosting its rate capability.[66–68]

3.2 Adsorption analysis

3.2.1 Effect of pH. pH affects both the adsorbent's surface charge and the adsorbate's speciation. Choosing a pH without justification may mask optimal adsorption conditions or ignore competitive interactions, as the adsorption efficiency can differ greatly across pH ranges for various systems.

The interaction of surface charge properties, electrostatic interactions, and CV pK_a values can be used to demonstrate the effective adsorption of CV onto SACs made from frankincense powder at the ideal pH of 8. Since electrostatic attraction is more common at pH 8, the activated carbon surface, which has a point of zero charge (pH_{pzc}) of 4.00, is negatively charged at this pH, which makes it easier for the positively charged CV ions (CV^+) to adsorb,[69] Fig. 4a. The pK_a values of CV (5.31 and 8.64)[70] indicate that at pH 8, CV primarily exists in its cationic form (CV^+), which is optimal for adsorption on the negatively charged surface of the SAC.[71,72] Protonation causes the surface of SAC to become positively charged, leading to electrostatic repulsion between the surface and CV^+ ions, limiting adsorption below pH 4.00.[73] At higher pH values, protons (H^+) and CV^+ ions compete less for surface sites, allowing more CV to adsorb. Adding oxygen-containing groups (such as –COOH and –OH) increases the surface area and reactivity of the SAC, producing additional adsorption sites and enhancing the effective binding of CV *via* electrostatic and possibly hydrogen bonding processes.[59,74,75] As a result, favorable electrostatic interactions, the cationic nature of the dye at this pH, reduced proton competition, and increased surface reactivity due to sulfuric acid functionalization contributed to the best CV adsorption at pH 8. There was no additional increase in removal efficiency above pH 8, which plateaued as the pH increased (Fig. 4b).

3.2.2 Effect of adsorbent dose. The adsorbent dosage affects both the removal efficiency and equilibrium capacity. Providing a justification for the selected dose aids in determining whether the system is operating optimally, sub-optimally, or saturated. The removal efficiency of CV onto SAC increased with increasing adsorbent dosage until 0.075 g, at which point no significant improvement was detected. The ideal dose is 0.075 g, which provides enough active sites for maximal dye clearance. Beyond this point, further increases in adsorbent dose result in surface site saturation, which means that adding more adsorbent does not significantly increase the adsorption capacity because the dye ions are spread across a broader surface area, diminishing the efficiency per unit mass (Fig. 4c).[59,60,73]

3.2.3 Application using real samples. The applicability of SACs as efficient adsorbents for the treatment of raw water samples contaminated with CV dye is illustrated in Fig. 4d. The effect of water type was investigated as a matrix factor in the removal of CV to evaluate the suitability of the prepared material for raw water treatment. SAC exhibited high removal efficiency for the investigated dye contaminants across all tested water types, including distilled water, tap water, raw groundwater, and secondary treated water, at a CV concentration of 5 ppm and the optimum adsorbent dose. These findings demonstrate that the material possesses high sensitivity and selectivity for CV removal, indicating its potential for commercial-scale applications and its suitability for purifying various types of raw water samples.

3.2.4 Adsorption kinetics. For the purpose of measuring kinetic performances, the important of contact time between the prepared material and the adsorption of CV in an aqueous solution was assessed in order to better understand equilibrium adsorption (Fig. 5).

The adsorption process reaches equilibrium in about 60 minutes, with rapid adsorption kinetics observed in the initial 5 to 35 minutes. During this early stage, adsorption is driven by electrostatic interactions that facilitate the transfer of crystal violet (CV) molecules to the internal binding sites of the adsorbent, where many active surface sites are available. As time progresses beyond 35 minutes, repulsive forces between CV molecules at the solid–liquid interface and those in the bulk solution slow their movement toward the fewer remaining

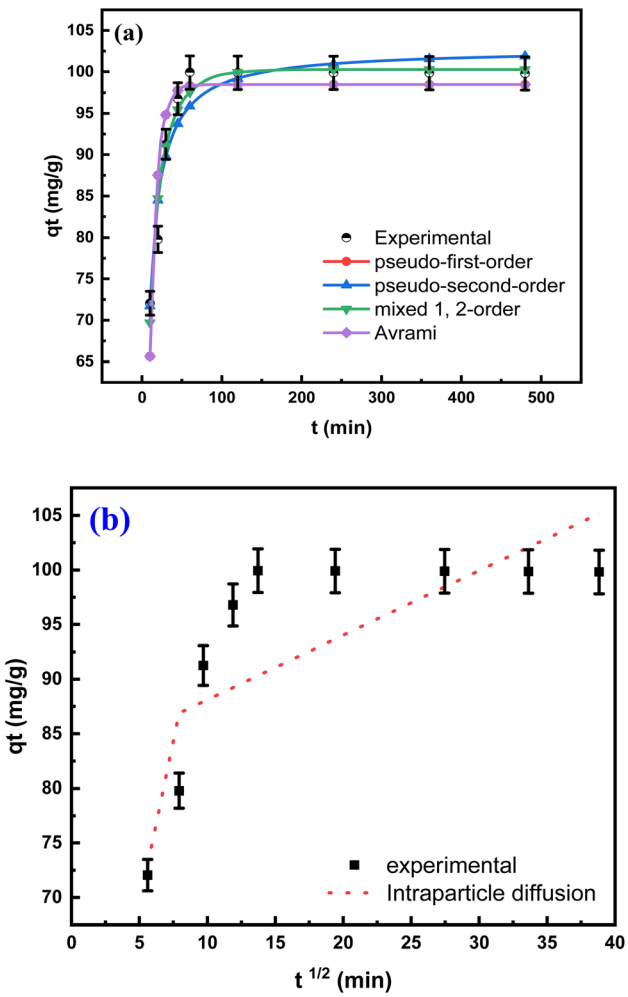

Fig. 5 Adsorption kinetic models of synthesized SAC for the removal of CV molecules.

active sites. Consequently, the adsorption rate decreases until equilibrium is achieved at around 60 minutes. After this point, diffusion of CV molecules is hindered due to the scarcity of unoccupied binding sites, resulting in a decline in adsorption efficacy as interactions between the adsorbent (SAC) and CV molecules weaken. Therefore, a contact time of one hour is optimal, as most adsorption occurs quickly within this period when abundant active sites are accessible. Following this, the rate gradually diminishes due to site saturation and reduced CV concentration in the solution. This kinetic behavior highlights the significance of surface site availability and electrostatic interactions in the adsorption mechanism.

To understand the rate-controlling mechanisms, the experimental data were fitted with several kinetic models. Interestingly, while multiple models (Pseudo-First-Order, Pseudo-Second-Order, Mixed-Order, and Avrami) showed high correlation coefficients ($R^2 > 0.99$), the Mixed 1,2-order model provided the best fit based on the lowest error functions. This suggests that the adsorption process is complex and not governed by a single mechanism, but rather involves a combination of physico–chemical interactions. The intraparticle diffusion model indicated that pore diffusion was not the sole rate-limiting step. The detailed parameters for all kinetic models are provided in Table S1 (SI). The fit to the Mixed-order model confirm the high efficiency of SAC for CV removal.[76]

3.2.5 Effect of temperature and thermodynamic study. When looking into the relationship between temperature and adsorption capacity, a direct correlation was found. CV's adsorption capacity increased with temperature, reaching its max at higher temperatures. Fig. 6a demonstrates that the removal % of CV increases with temperature, implying that the adsorption process is endothermic. The kinetic energy of the adsorbent and adsorbate increases with temperature, allowing dye molecules to overcome the energy barrier and adsorb onto the SAC surface.

The temperature range used in this investigation was 25–55 °C. To characterize the thermodynamic parameters of the adsorption process, the Gibbs free energy change (ΔG°) was calculated using the enthalpy (ΔH°) and entropy (ΔS°) values from a plot of $\ln K_d$ *vs.* $1/T\,(K^{-1})$. Fig. 6a and b illustrates how the van't Hoff eqn (4) was used to calculate the adsorption equilibrium constant ($K_d = (q_e/c_e)$) at different temperatures, thereby elucidating the adsorption mechanism.

$$\ln K_d = \Delta S^\circ/R - \Delta H^\circ/RT \quad (4)$$

where, K_d: the equilibrium constant (L mg^{-1}), R: is the gas rate constant (8.314 J mol^{-1} K^{-1}), ΔH°: the enthalpy change of adsorption (kJ mol^{-1}), ΔS°: the entropy of adsorption, and Gibbs free energy (ΔG°). Eqn (5) and (6) can be used to compute the equilibrium constant (K_d) (L mg^{-1}), gas rate constant (R) (8.314 J mol^{-1} K^{-1}), enthalpy change of adsorption (kJ mol^{-1}), entropy of adsorption (ΔS°), and Gibbs free energy (ΔG).

$$\Delta G^\circ = -RT \ln K_d = \Delta H^\circ - T\Delta S^\circ \quad (5)$$

$$\ln K_d = -\Delta H^\circ/R\,(1/T) + \Delta S^\circ/R \quad (6)$$

Table S2 shows negative values for ΔG°, ΔH°, and ΔS°, indicating an exothermic, nonspontaneous adsorption process for CV.

3.2.6 Adsorption isotherm. The equilibrium adsorption data were analyzed using various isotherm models to elucidate the distribution of CV molecules between the liquid and solid phases. The analysis revealed that the experimental data were well-described by several two- and three-parameter models, as shown in Fig. 7. However, a comprehensive error function

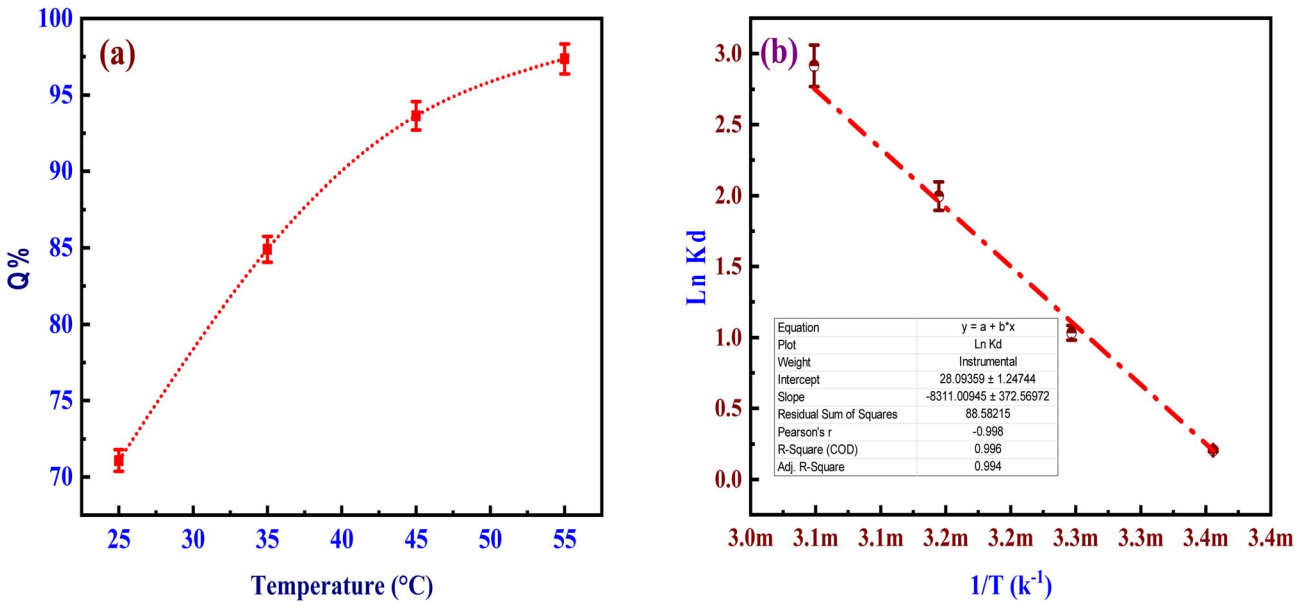

Fig. 6 (a) Effect of temperature on the adsorption of CV onto the SAC and (b) van't Hoff plot.

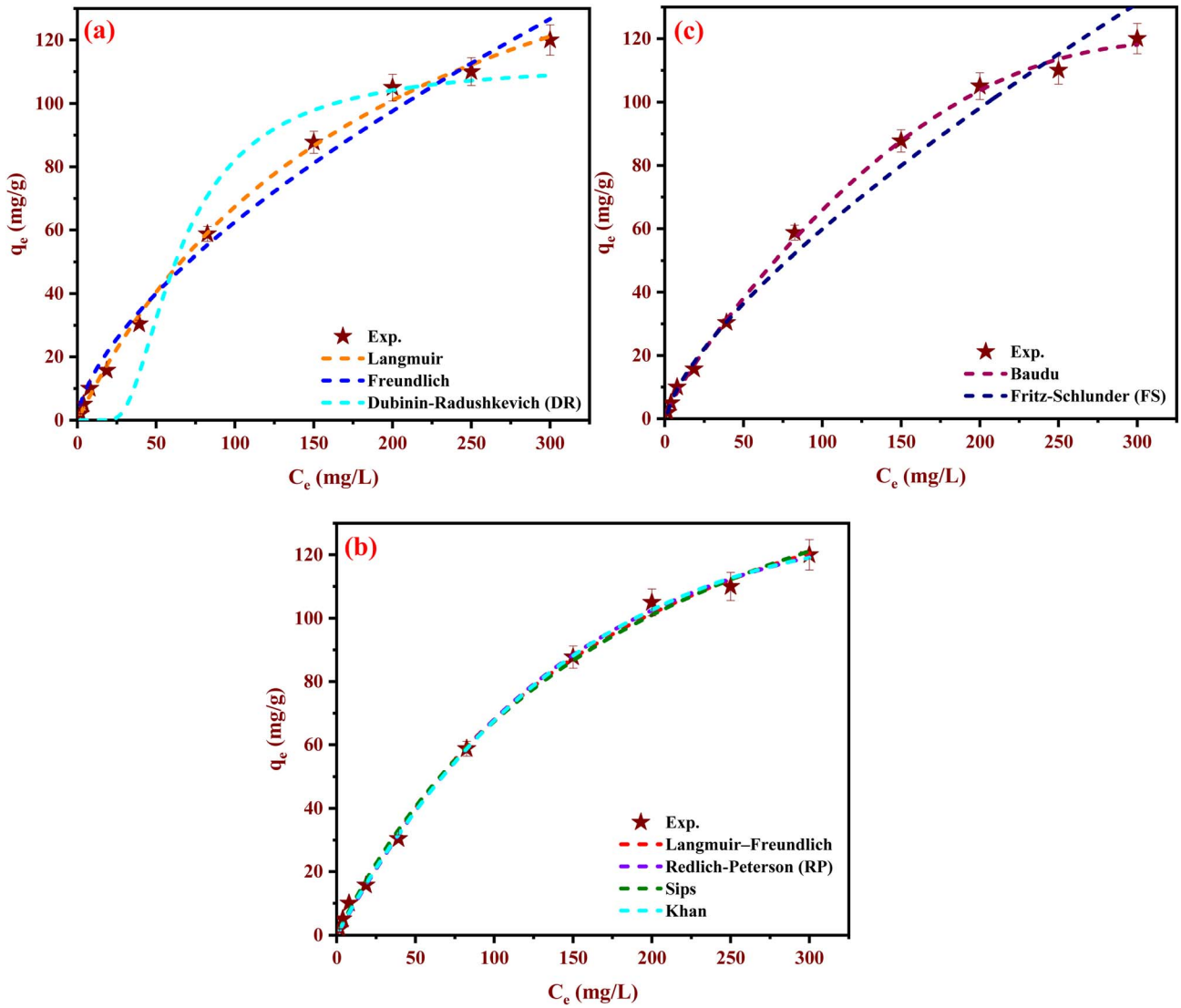

Fig. 7 Isotherm models of SAC for the removal of CV.

analysis (detailed in Table S3 and S4) was conducted to identify the most appropriate model.

The Fritz–Schlunder (five-parameter)[77] and Redlich–Peterson (three-parameter) isotherms[78] provided the best fit to the experimental data, as indicated by their highest R^2 values (0.999) and the lowest error metrics across all functions. This indicates a complex adsorption process on a heterogeneous surface. The maximum adsorption capacity (q_{max}) derived from the Langmuir–Freundlich model,[79] which also showed an excellent fit, was 638.51 mg g^{-1}, underscoring the superior performance of the SAC adsorbent compared to many other materials[80] (see Table 1).

3.3 Analysis of response surfaces and experimental design modeling

3.3.1 Examining statistics. The Box–Behnken Design (BBD) was employed to systematically optimize the critical parameters including initial CV concentration (A), contact time (B), adsorbent dose (C), and pH (D) for maximizing adsorption efficiency. The complete experimental design matrix and results are provided in SI (Table S5). A highly significant ($p < 0.0001$) quadratic model was developed, which exhibited an excellent fit to the experimental data ($R^2 = 0.9995$). The detailed Analysis of Variance (ANOVA) is summarized in SI (Tables S6–S8). The model in terms of coded factors is presented in eqn (7), which allows for direct comparison of the factor effects based on the magnitude of the coefficients:

$$R = 81.9 - 25.77A + 25.08B + 5.28C + 14.86D + 2.03AD - 13.87A^2 - 18.94B^2 - 6.58D^2 \quad (7)$$

where A: initial concentration, B: contact time, C: adsorbent dose, D: pH.

The three-dimensional response surface plots (Fig. 8) visualize the interactive effects of these variables on the CV removal percentage.

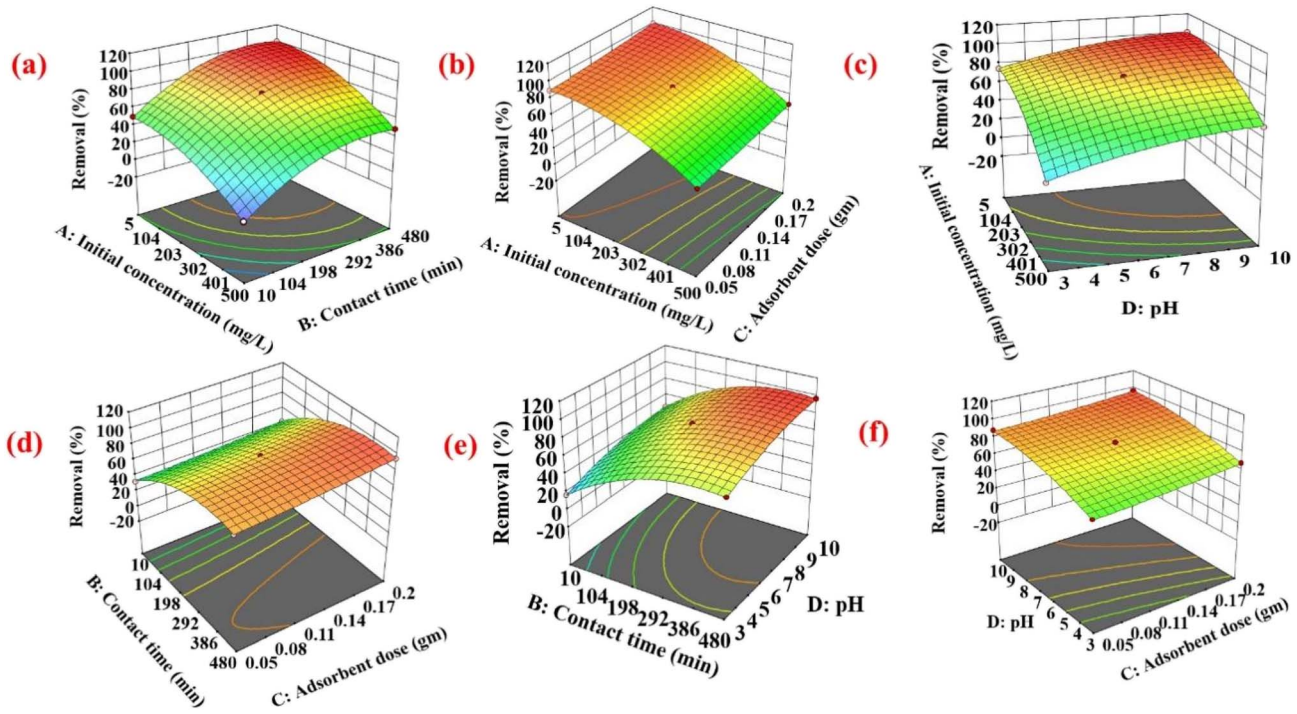

Fig. 8 Optimization plots for CV adsorption: (a) removal % *vs.* initial concentration and contact time, (b) removal % *vs.* initial concentration and adsorbent dose, (c) removal % *vs.* initial concentration and pH, (d) removal % *vs.* contact time and adsorbent dose, (e) removal % *vs.* contact time and pH, and (f) removal % *vs.* adsorbent dose and pH.

The interaction between initial CV concentration and contact time is shown in Fig. 8a. A clear inverse relationship was observed between concentration and removal efficiency, attributable to the saturation of finite adsorption sites on the SAC at higher dye loadings. In contrast, longer contact times consistently improved efficiency by facilitating greater diffusion and interaction of CV molecules with the adsorbent surface.

Fig. 8b illustrates the effect of adsorbent dosage and initial concentration. Higher adsorbent doses provided a greater abundance of active sites, which significantly enhanced removal performance, even at elevated dye concentrations.[76,81] The critical role of pH is evident in its interactions with other factors. Fig. 8c (pH *vs.* initial concentration) and Fig. 8e (pH *vs.* contact time) demonstrate that basic conditions are essential for high efficiency. As established in Section 3.2.1, at a solution pH above the point of zero charge ($pH_{pzc} = 4.0$), the SAC surface becomes negatively charged, enabling strong electrostatic attraction with the cationic CV molecules. The extensive plateau regions observed in these response surfaces are particularly advantageous, indicating a robust process where minor fluctuations in pH around the optimum will not significantly compromise performance.

The interaction between contact time and adsorbent dose (Fig. 8d) revealed that high efficiency could be achieved with a minimal dose of 0.05 g and a contact time of 60 minutes, underscoring the high intrinsic capacity of the SAC material. Finally, the relationship between adsorbent dose and pH (Fig. 8f) further confirmed that the optimal adsorption occurred at a pH of 8 across all tested doses.

Numerical optimization based on the model predicted a maximum CV removal efficiency of 98.63% under the following optimal conditions: initial concentration of 80.96 mg L^{-1}, contact time of 247.40 min, adsorbent dose of 0.103 g, and solution pH of 9.36.[14,23]

3.3.2 Model adequacy checking. The model's high reliability is illustrated in Fig. 9a, where the residual points align in a straight-line pattern on the normal probability plot, demonstrating the model's sufficiency. The model's accuracy in maximizing dye removal efficiency is further supported by Fig. 9b, which shows the anticipated *vs.* real values with data points dispersed randomly around the 45° reference line. Another essential diagnostic tool for determining whether data transformation is necessary is the Box–Cox transformation chart. This approach also provides information on how to select the optimal power-law transformation by utilizing the lambda value. As shown in Fig. 9c, the Box–Cox plot displays the converted residuals against the lambda values. It was discovered that 2.69302 was the optimal lambda for CV removal. Furthermore, as shown in Fig. 9c, the lambda value of the present model was determined to be 1.[81] These findings suggest that, without considering the necessity of data transformation, the current power structure is already optimal. The residual plot against the data from the experimental run is displayed in Fig. 9d. The random distribution of the residuals demonstrates the statistical robustness of the model and its applicability for predicting CV removal efficiency. The accuracy of the model is confirmed by the high correlation between the experimental and projected adsorption capacities in Fig. 9e. In conclusion,

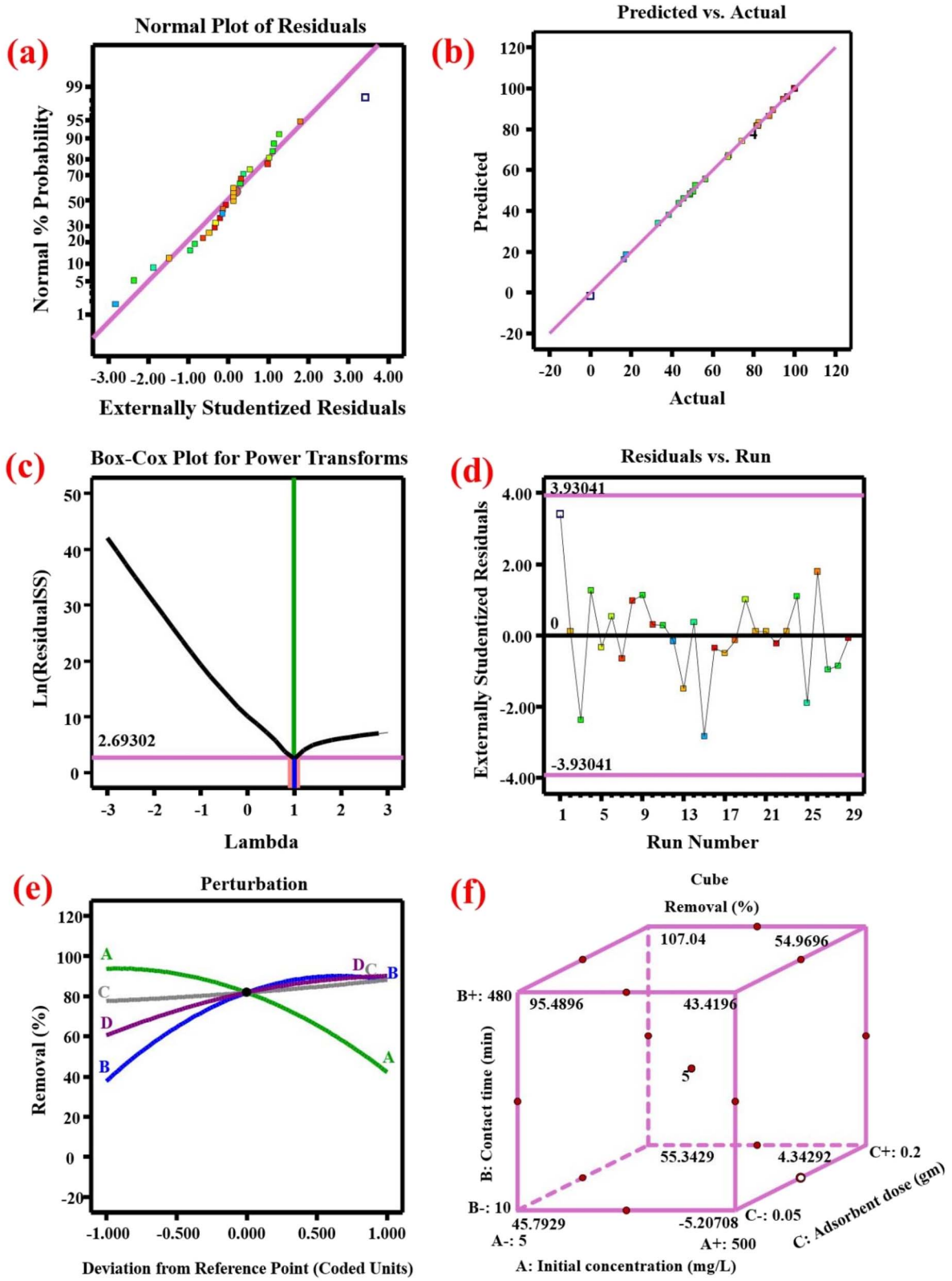

Fig. 9 Shows the normal residual probability (a), definite values *versus* predicted values (b), Box–Cox plot power transform (c), residual *versus* run (d), perturbation of adsorption CV onto activated carbon (for *A*: initial CV concentration, *B*: contact time, *C*: dose, and *D*: pH), and graphic optimization of the CV adsorption capability (f).

the following conditions were determined to be optimal for CV adsorption onto activated carbon: a pH of 9.363 for the solution, an initial concentration of 80.9588 mg L^{-1}, a contact time of 247.402 minutes, and an adsorbent dosage of 0.102958 g. These ideal conditions are illustrated graphically in Fig. 9f. The adsorption process was found to be highly effective under these circumstances, as evidenced by the expected adsorption efficiency of 98.6284%.[82,83]

3.4 Volarization of spent adsorption in methanol oxidation

Embracing a circular economy approach, the CV-laden spent adsorbent (SAC/CV) was repurposed as an electrocatalyst for the methanol oxidation reaction (MOR), a critical anodic process in direct methanol fuel cells (DMFCs).

3.4.1 Electrocatalytic performance and mechanism. In an alkaline DMFC, the overall goal of the MOR is the complete oxidation of methanol to carbonate, facilitating electricity generation. The intended overall reaction is illustrated in eqn 8:

$$CH_3OH + 8OH^- \rightarrow CO_3^{2-} + 6H_2O + 6e^- \quad (8)$$

This process typically proceeds through a complex mechanism involving multiple electron transfers and adsorbed intermediates (*e.g.*, CO), which can poison the catalyst surface. The electrocatalytic activity of the SAC and spent SAC/CV electrodes was evaluated using cyclic voltammetry. Fig. 10a and b depicts the cyclic voltammograms at a fixed scan rate of 50 mV s^{-1} with varying methanol concentrations (0.5–2.0 M). The current density increased with methanol concentration up to 1.5 M, beyond which it plateaued, indicating saturation or the onset of catalyst poisoning by intermediate species.[84]

3.4.2 Electrochemical kinetics and stability. The electrochemical kinetics were further investigated by analyzing the scan rate dependence. Fig. 10c and d shows the cyclic voltammetric curves for SAC and SAC/CV electrodes at scan rates from 10 to 100 mV s^{-1}. The linear increase in peak current density with the square root of the scan rate (not shown) suggested a diffusion-controlled process. A comparison of the electrodes at the optimal methanol concentration (Fig. 10 e) revealed that the pristine SAC achieved a superior peak current density of 22.40 mA cm^{-2}, compared to 20.55 mA cm^{-2} for the spent SAC/CV. This decrease is likely due to the partial blockage of active sites by adsorbed CV molecules. Chronoamperometry studies confirmed a gradual current decay over 3600 seconds, which is characteristic of MOR catalysts undergoing progressive poisoning by reaction intermediates.

3.5 Greenness and applicability assessment

The environmental sustainability and practical applicability of the proposed SAC-based adsorption method were evaluated using a suite of quantitative green chemistry metrics.[85–87] The assessment employed the Analytical Eco-Scale, the AGREE calculator[87] (based on the 12 principles of green analytical chemistry), and the Blue Applicability Grade Index (BAGI).

The results, consolidated in Fig. 11, demonstrate that the process is both environmentally friendly and practically viable. The method achieved an excellent Analytical Eco-Scale score of 90 out of 100 (Table 3), indicating minimal environmental

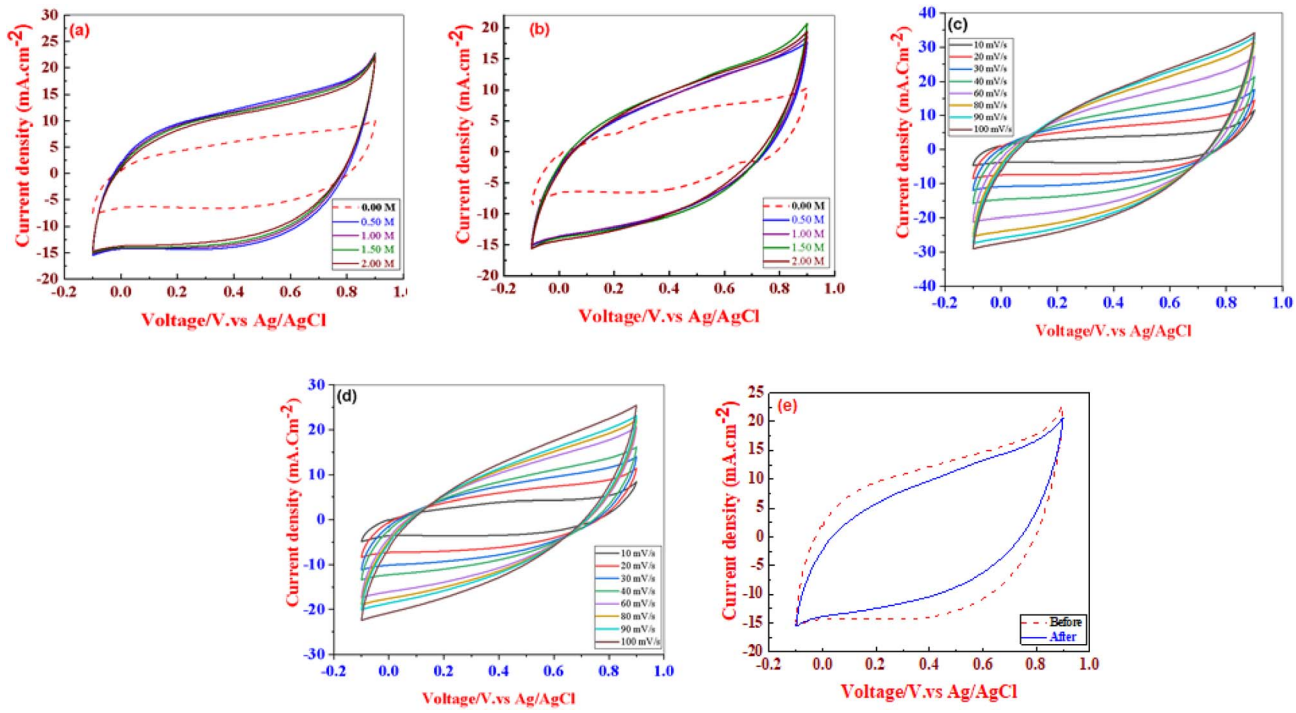

Fig. 10 Electrocatalytic evaluation for methanol oxidation: cyclic voltammetric curves for (a) SAC and (b) SAC/CV at varying methanol concentrations (0–2 M) at 50 mV s^{-1}. Scan rate dependence for (c) SAC and (d) SAC/CV from 10 to 100 mV s^{-1}. (e) Direct comparison of SAC and SAC/CV electrodes at the optimal methanol concentration.

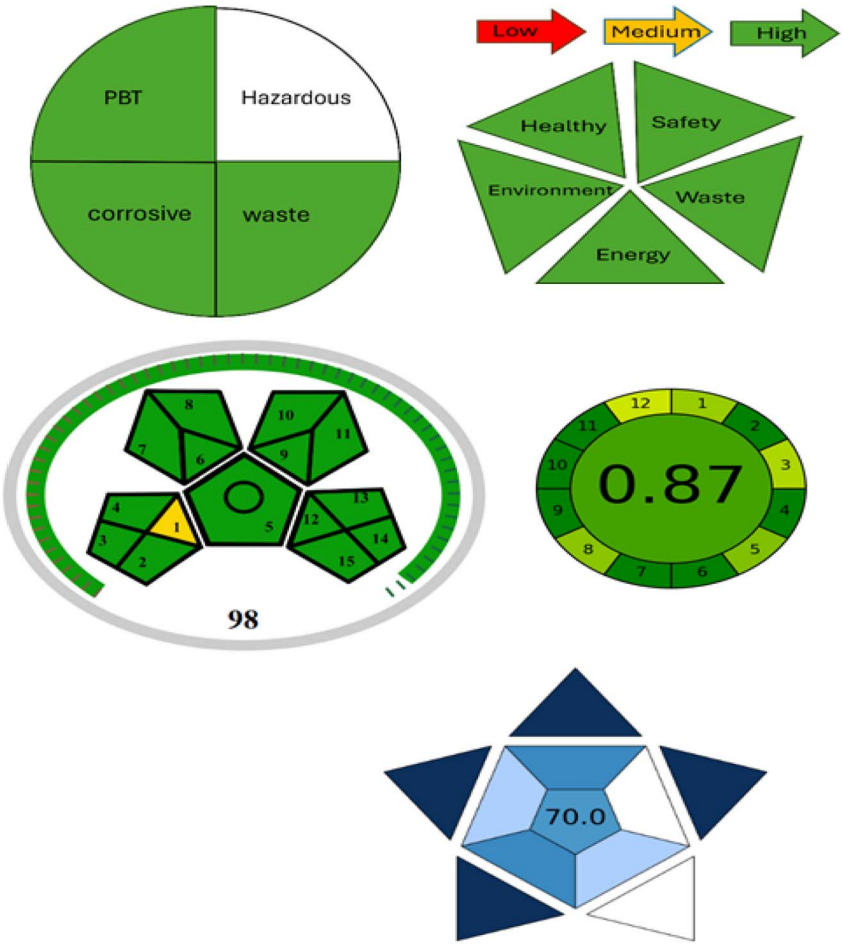

Fig. 11 Integrated green chemistry and applicability profile. The assessment shows (a) an AGREE score of 0.84, indicating excellent greenness; (b) a BAGI score of 70, reflecting high practical applicability; and (c) an Analytical Eco-Scale score of 90/100, confirming a low environmental impact.

Table 3 Shows the penalty points (PPs) of the suggested method on the basis of the analytical eco-scale

Analytical eco-scale		
Reagents	Methanol	1
	Sulphuric acid	3
	Sodium hydroxide	2
Instruments	Oven	2
	UV-VIS spectrometry	0
	XRD	2
	Total PP	10
	Eco-scale	90

impact. The AGREE assessment yielded a high score of 0.84, confirming strong adherence to green chemistry principles across multiple criteria. Furthermore, the BAGI tool awarded a strong applicability score of 70, highlighting the method's robustness, cost-effectiveness, and potential for implementation in routine analysis.

This multi-faceted evaluation confirms that the SAC adsorption process is not only effective for CV removal but also aligns with the principles of green chemistry and demonstrates high practical utility.

3.6 Cost analysis and economic feasibility

The economic viability of the SAC adsorbent is a critical factor for its potential scale-up and practical application. A detailed cost analysis for the production of the sulfuric acid-functionalized activated carbon was performed. The total manufacturing cost was calculated to be approximately $0.064 per gram of SAC, confirming its potential as a cost-effective solution for wastewater treatment. The complete breakdown of material and energy costs is provided in Table S9.

3.7 Adsorption mechanism

Porous SACs may adsorb organic dyes, including CV cationic dyes, through several methods including as hydrogen bonding, π–π stacking, pore diffusion, and electrostatic forces. Fig. 12 displays the most common interactions that lead to CV adsorption. The SAC's mesoporous structure contains fewer micropores (average pore width = 3.0 nm) than the CV dye, with a molecular size of 1.4 nm.[88] As a result, the SAC's micropores

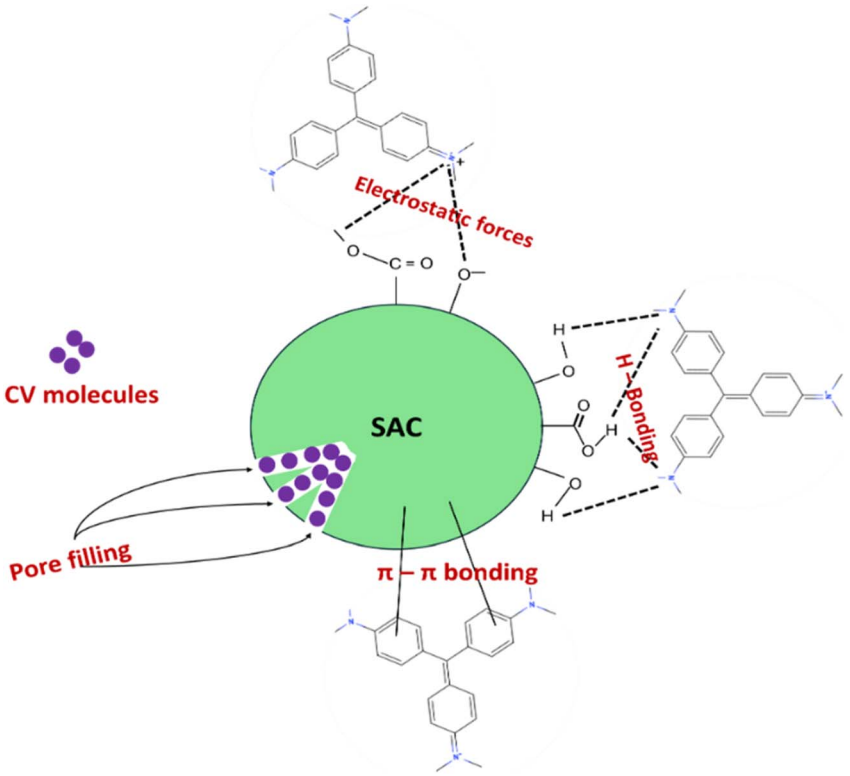

Fig. 12 Diagrammatic illustration of the suggested CV dye adsorption mechanism upon SAC.

and mesopores fill up with CV dye molecules. The observed data (CV adsorption) show that the CV dye uptake took place in a basic environment (pH > pH_{pzc}). In this medium, SACs' functional groups, or active sites, such as $-O^-$ and $-COO^-$ become negatively charged. As a result, positively charged groups in CV dye molecules can electrostatically interact

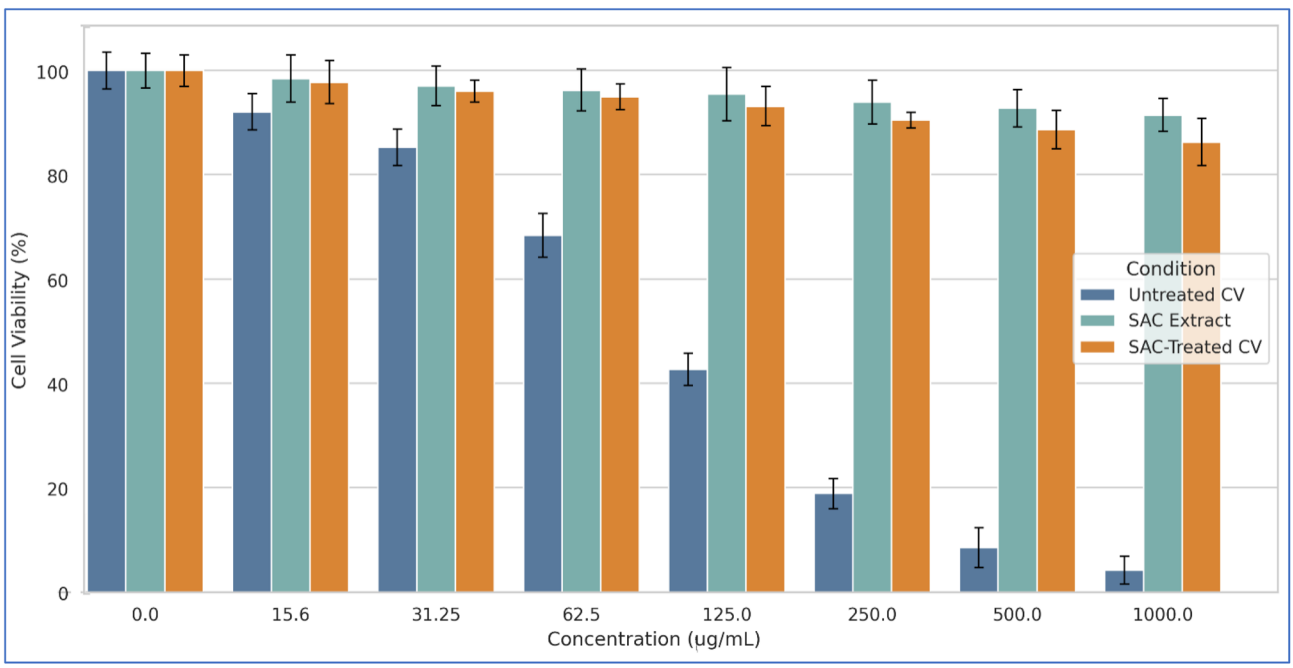

Fig. 13 Cell viability in HepG2 cells across increasing sample concentrations following 72-hour exposure across a concentration range of 0–1000 μg mL^{-1} to evaluate the maximum cytotoxic effect for three conditions: untreated CV, SAC extract, and SAC-treated CV. Bars represent mean viability (%) and error bars indicate standard deviation. SAC preserves high viability across all concentrations and markedly attenuates the concentration-dependent cytotoxicity observed in untreated CV, with SAC-treated CV tracking closely to SAC alone.

with negatively charged functional groups on the adsorbent surface. In addition, the H atoms of the O-containing functional groups on the SAC surface can form hydrogen bonds with the CV species' N atoms. SAC's hexagonal structure and CV's benzene rings improve adsorption effectiveness by acting as electron donors and acceptors through a process called π–π stacking.[89]

3.8 Biological safety assessment

3.8.1 Cytotoxicity evaluation using MTT assay. The cytotoxic effects of untreated crystal violet (CV), SAC extract, and SAC-treated CV solutions on HepG2 human hepatocellular carcinoma cells were systematically evaluated using the MTT assay over multiple exposure periods. Fig. 13 presents the cell viability data following 72-hour exposure across a concentration range of 0–1000 μg mL^{-1}.

Untreated CV solutions demonstrated pronounced concentration-dependent cytotoxicity against HepG2 cells. At low concentrations (0–31.25 μg mL^{-1}), cell viability remained relatively high, ranging from 100% at baseline to approximately 85% at 31.25 μg mL^{-1}. However, a sharp decline in viability was observed at higher concentrations, with cell viability dropping to 68% at 62.5 μg mL^{-1}, 44% at 125 μg mL^{-1}, and reaching critically low levels of 19% and 10% at 250 μg mL^{-1} and 500 μg mL^{-1}, respectively. At the highest tested concentration (1000 μg mL^{-1}), cell viability was reduced to approximately 5%, indicating severe cytotoxic effects. The calculated half-maximal cytotoxic concentration (C_{50}) was determined to be 84.7 μg mL^{-1}.

In contrast to untreated CV, SAC extract demonstrated excellent biocompatibility across all tested concentrations. Cell viability remained consistently high, ranging from 98–100% at low concentrations (0–62.5 μg mL^{-1}) and showing only minimal decreases at higher concentrations, maintaining 95% viability at 250 μg mL^{-1}, 93% at 500 μg mL^{-1}, and 90% at 1000 μg mL^{-1}. The narrow error bars and consistently high viability values indicate that SAC extract poses minimal cytotoxic risk to human hepatocellular cells.

Most significantly, SAC-treated CV solutions exhibited a cytotoxicity profile nearly identical to that of SAC extract alone, demonstrating the remarkable detoxification capacity of the treatment process. Cell viabilities for SAC-treated solutions closely tracked those of SAC extract across all concentrations: 98% at 15.6 μg mL^{-1}, 96% at 31.25 μg mL^{-1}, 95% at 62.5 μg mL^{-1}, 93% at 125 μg mL^{-1}, 91% at 250 μg mL^{-1}, 88% at 500 μg mL^{-1}, and 85% at 1000 μg mL^{-1}. The statistical overlap between SAC extract and SAC-treated CV viability curves, as evidenced by overlapping error bars, confirms the effective neutralization of CV cytotoxicity.

The biological safety assessment reveals critical insights into both the environmental hazards posed by crystal violet contamination and the protective efficacy of SAC treatment. The severe concentration-dependent cytotoxicity observed with untreated CV solutions underscores the significant health risks associated with exposure to this synthetic dye, particularly at concentrations commonly found in industrial effluents.

The excellent biocompatibility profile of SAC extract validates its suitability for water treatment applications. The minimal cytotoxicity observed even at high concentrations (1000 μg mL^{-1}) demonstrates that potential leaching of bioactive compounds from the adsorbent poses negligible health risks. This finding is particularly important for practical applications where complete adsorbent recovery may be challenging, as residual SAC particles in treated water would not contribute to cytotoxic effects.

These findings have profound implications for environmental remediation and public health protection. The ability of SAC treatment to transform highly cytotoxic CV solutions into biocompatible effluents demonstrates its potential for treating industrial wastewater containing synthetic dyes. The maintenance of cell viability above 85% even at the highest tested concentrations suggests that SAC-treated water could meet stringent safety standards for various discharge or reuse applications.

The dramatic difference in cytotoxicity profiles between untreated and treated solutions (*e.g.*, 10% *vs.* 88% viability at 500 μg mL^{-1}) quantifies the risk reduction achieved through SAC treatment. This >8-fold improvement in biological safety at high concentrations demonstrates the critical importance of implementing effective treatment technologies for dye-containing effluents.

4 Conclusion

This work shows that Sulphuric acid-functionalized activated carbon produced from frankincense may effectively remove crystal violet color from aqueous solutions. The adsorption process was thoroughly optimised using response surface methods, demonstrating favorable interactions between dye molecules, the porous structure, and the adsorbent's surface functional groups. Kinetic and equilibrium studies provided insights into the adsorption mechanism, whereas thermodynamic analysis characterized the nature of the process. The material showed promising potential for reuse in electrochemical applications, particularly in methanol oxidation reactions. A comprehensive green chemistry assessment confirmed the environmental sustainability of the approach. These findings suggest that this biomass-derived adsorbent offers a viable solution for wastewater treatment, combining effective contaminant removal with potential material valorization. Further research could explore scale-up possibilities and applications in complex wastewater matrices to enhance practical implementation.

List of abbreviations

AC	Activated Carbon
AGP	Analytical Greenness Profile
AGREE	Analytical Greenness Calculator
BBD	Box–Behnken Design
BAGI	Blue Applicability Grade Index
CV	Crystal Violet
FT-IR	Fourier Transform Infrared Spectroscopy

HepG2	Human Hepatocellular Carcinoma Cell Line
Mo GAPI	Modified Green Analytical Procedure Index
NEMI	National Environmental Methods Index
RP-HPLC	Reverse-Phase High-Performance Liquid Chromatography
SAC	Sulfuric Acid–Functionalized Activated Carbon
SEM	Scanning Electron Microscope
XRD	X-Ray Diffraction

Consent for publication

The authors confirm:

- This work represents original research that has not been previously published in any form;
- This manuscript has not been submitted for review or publication consideration elsewhere;
- The publication has received approval from all coauthors.

Ethics approval and consent to participate

Not applicable, as the study did not apply to human or animal studies. The article does not include any studies on human participants or animals conducted by any of the authors.

Conflicts of interest

All the authors declare that they have no conflicts of interest to disclose.

Data availability

The datasets generated and/or analyzed during this study are available from the corresponding author upon reasonable request.

Supplementary information is available. See DOI: **https://doi.org/10.1039/d5ra07463k**.

Acknowledgements

This work was supported and funded by the Deanship of Scientific Research at Imam Mohammad Ibn Saud Islamic University (IMSIU) (grant number IMSIU-DDRSP2501).

References

1 B. S. Rathi, P. S. Kumar and D.-V. N. Vo, *Sci. Total Environ.*, 2021, **797**, 149134.
2 A. Waheed, N. Baig, N. Ullah and W. Falath, *J. Environ. Manage.*, 2021, **287**, 112360.
3 R. A. Schnick, *Prog. Fish-Cult.*, 1988, **50**, 190–196.
4 J. Sharma, S. Sharma and V. Soni, *Reg. Stud. Mar. Sci.*, 2021, **45**, 101802.
5 S. Dutta, S. Adhikary, S. Bhattacharya, D. Roy, S. Chatterjee, A. Chakraborty, D. Banerjee, A. Ganguly, S. Nanda and P. Rajak, *J. Environ. Manage.*, 2024, **353**, 120103.
6 S. Senthilkumaar, P. Kalaamani and C. V Subburaam, *J. Hazard. Mater.*, 2006, **136**, 800–808.
7 K. P. Singh, S. Gupta, A. K. Singh and S. Sinha, *J. Hazard. Mater.*, 2011, **186**, 1462–1473.
8 N. Hemashenpagam and S. Selvajeyanthi, in *Nanohybrid Materials for Treatment of Textiles Dyes*, Springer, 2023, pp. 41–60.
9 G. Kaur, S. Bera and J. Emerg, *Technol. Innov. Res.*, 2020, **7**, 174–183.
10 Z. Falaki and H. Bashiri, *J. Iran. Chem. Soc.*, 2021, **18**, 2689–2702.
11 J.-S. Wu, C.-H. Liu, K. H. Chu and S.-Y. Suen, *J. Membr. Sci.*, 2008, **309**, 239–245.
12 H. Bashiri and M. Rafiee, *J. Saudi Chem. Soc.*, 2016, **20**, 474–479.
13 K. Azam, N. Shezad, I. Shafiq, P. Akhter, F. Akhtar, F. Jamil, S. Shafique, Y.-K. Park and M. Hussain, *Chemosphere*, 2022, **306**, 135566.
14 D. Lan, H. Zhu, J. Zhang, S. Li, Q. Chen, C. Wang, T. Wu and M. Xu, *Chemosphere*, 2022, **293**, 133464.
15 A. L. Cukierman, G. V Nunell and P. R. Bonelli, in *Emerging and Nanomaterial Contaminants in Wastewater*, Elsevier, 2019, pp. 159–213.
16 H. H. Shah, M. Amin, F. Pepe, E. Mancusi and A. G. Fareed, *Environ. Sci. Pollut. Res.*, 2025, **32**, 19084–19109.
17 S. Basar, *Staats-und Universitätsbibliothek Hamburg Carl von Ossietzky*, 2005.
18 S. I. Abdelwahab, M. M. E. Taha, A. A. Jerah, A. Farasani, S. M. Abdullah, I. A. Aljahdali, O. Oraibi, B. Oraibi, H. A. Alfaifi and A. H. Alzahrani, *Heliyon*, 2024, **10**(19), e38102.
19 M. Danish and T. Ahmad, *Renew. Sustain. Energy Rev.*, 2018, **87**, 1–21.
20 N. A. Rashidi, Y. H. Chai, I. S. Ismail, M. F. H. Othman and S. Yusup, *Biomass Convers. Biorefinery*, 2022, 1–15.
21 Y. Liu and X. Zhang, *Electrochim. Acta*, 2009, **54**, 4180–4185.
22 M. Kashif, C. Kang, T. R. Siddhartha, C. A. Che, Y. Su and P. M. Heynderickx, *Vacuum*, 2024, 113415.
23 A. Elmouwahidi, J. Castelo-Quibén, J. F. Vivo-Vilches, A. F. Pérez-Cadenas, F. J. Maldonado-Hódar and F. Carrasco-Marín, *Chem. Eng. J.*, 2018, **334**, 1835–1841.
24 R. Xing, Y. Liu, Y. Wang, L. Chen, H. Wu, Y. Jiang, M. He and P. Wu, *Microporous Mesoporous Mater.*, 2007, **105**, 41–48.
25 T. S. Gaaz, A. B. Sulong, A. A. H. Kadhum, M. H. Nassir and A. A. Al-Amiery, *Materials*, 2016, **9**, 620.
26 N. Bhagwandin, T. Mdlazi, K. Sanaullah, M. R. Rahman, A. H. Mohammadi and M. K. Bin Bakri, *Int. J. Environ. Anal. Chem.*, 2025, 1–20.
27 S. Hanif, N. Iqbal, T. Noor, N. Zaman and K. Vignarooban, *Sci. Rep.*, 2021, **11**, 17192.
28 A. Naeimi, M.-S. Ekrami-Kakhki and F. Donyagard, *Int. J. Hydrogen Energy*, 2021, **46**, 18949–18963.
29 S. Sheikhi and F. Jalali, *Int. J. Hydrogen Energy*, 2021, **46**, 10723–10738.
30 Z. Wang, H. Jin, T. Meng, K. Liao, W. Meng, J. Yang, D. He, Y. Xiong and S. Mu, *Adv. Funct. Mater.*, 2018, **28**, 1802596.

31 T. O. Report, D. S. Tong, F. E. Soetaredjo, A. Ayucitra, W. H. Yu, Y. Liu, Y. Gu, S. Liu, G. Zeng, X. Cai, H. Wang, S. Liu, S. Meon, M. H. Musa, A. K. Rahardjo, M. Josephine, J. Susanto, A. Kurniawan, A. Benhouria and M. Boutahala, *J. Environ. Chem. Eng.*, 2018, 1–25.
32 A. Adak, M. Bandyopadhyay and A. Pal, *Sep. Purif. Technol.*, 2005, **44**, 139–144.
33 E. Y. Santali, I. A. Naguib, A. M. Alshehri, Y. A. Alzahrani, A. E. Alharthi, T. S. Alosaimi, B. D. Alsayali, I. Alsalahat, A. Almahri and M. A. S. Abourehab, *Separations*, 2022, **9**, 275.
34 P. L. Homagai, R. Poudel, S. Poudel and A. Bhattarai, *Heliyon*, 2022, **8**, e09261.
35 H. J. Kumari, P. Krishnamoorthy, T. K. Arumugam, S. Radhakrishnan and D. Vasudevan, *Int. J. Biol. Macromol.*, 2017, **96**, 324–333.
36 M. Hussain, S. S. Hussaini, M. Shariq, N. AlMasoud, G. A. AlZaidy, K. F. Hassan, S. K. Ali, R. E. Azooz, M. A. Siddiqui and K. Seku, *ACS Omega*, 2024, **9**, 11459–11470.
37 W. Liu, R. Guo, G. Peng and D. Yin, *Nanomaterials*, 2022, **12**, 1462.
38 E. C. Souza Junior, M. P. F. Santos, J. B. Santos, R. G. dos Santos, M. J. P. Brito, R. C. F. Bonomo and C. M. Veloso, *Biochem. Eng. J.*, 2025, **223**, 109888.
39 N. Jayarambabu, N. V. S. S. S. Rao, M. K. C. Sivalenka, K. Saraswathi, B. S. Naick, N. Anitha and T. V. Rao, *Diam. Relat. Mater.*, 2024, **144**, 110959.
40 G. Kathiresan, K. Vijayakumar, A. P. Sundarrajan, H. S. Kim and K. Adaikalam, *Optik*, 2021, **238**, 166671.
41 S. Senthilkumaar, P. R. Varadarajan, K. Porkodi and C. V Subbhuraam, *J. Colloid Interface Sci.*, 2005, **284**, 78–82.
42 W. Rudzinski and W. Plazinski, *Environ. Sci. Technol.*, 2008, **42**, 2470–2475.
43 M. Avrami, *J. Chem. Phys.*, 1941, **9**, 177–184.
44 J. Serafin and B. Dziejarski, *Microporous Mesoporous Mater.*, 2023, **354**, 112513.
45 G. A. A. Al-Hazmi, A. A. El-Zahhar, M. G. El-Desouky, M. A. El-Bindary and A. A. El-Bindary, *J. Coord. Chem.*, 2022, **75**, 1203–1229.
46 G. A. A. Al-Hazmi, A. A. El-Zahhar, M. G. El-Desouky and A. El-Bindary, *Environ. Technol.*, 2024, **45**, 1969–1988.
47 G. A. A. Al-Hazmi, M. A. El-Bindary, M. G. El-Desouky and A. A. El-Bindary, *Desalin. Water Treat.*, 2022, **258**, 85–103.
48 G. A. A. M. Al-Hazmi, A. A. Alayyafi, M. G. El-Desouky and A. A. El-Bindary, *Int. J. Biol. Macromol.*, 2024, **262**, 129995.
49 G. A. A. M. Al-Hazmi, A. A. Alayyafi, M. G. El-Desouky and A. A. El-Bindary, *Int. J. Biol. Macromol.*, 2024, **261**, 129769.
50 G. A. A. Al-Hazmi, A. A. El-Zahhar, M. G. El-Desouky, M. A. El-Bindary and A. A. El-Bindary, *Environ. Technol.*, 2024, **45**, 731–750.
51 M. Sajid and J. Płotka-Wasylka, *Talanta*, 2022, **238**, 123046.
52 M. Marć, W. Wojnowski, F. Pena-Pereira, M. Tobiszewski and A. Martín-Esteban, *ACS Sustain. Chem. Eng.*, 2024, **12**, 12516–12524.
53 N. Manousi, W. Wojnowski, J. Płotka-Wasylka and V. Samanidou, *Green Chem.*, 2023, **25**, 7598–7604.
54 L. Yin, L. Yu, Y. Guo, C. Wang, Y. Ge, X. Zheng, N. Zhang, J. You, Y. Zhang and M. Shi, *J. Pharm. Anal.*, 2024, 101013.
55 F. Wang, X. Qi, H. Zhang and Z. Yang, *Carbon N. Y.*, 2025, 119999.
56 S. Shin, J. Jang, S.-H. Yoon and I. Mochida, *Carbon N. Y.*, 1997, **35**, 1739–1743.
57 S. Biniak, G. Szymański, J. Siedlewski and A. Świątkowski, *Carbon N. Y.*, 1997, **35**, 1799–1810.
58 T. S. Malarvizhi and T. Santhi, *Res. Chem. Intermed.*, 2013, **39**, 2473–2494.
59 M. K. Uddin, N. N. Abd Malek, A. H. Jawad and S. Sabar, *Int. J. Phytoremediation*, 2023, **25**, 393–402.
60 A. S. Yusuff, O. A. Ajayi and L. T. Popoola, *Sci. African*, 2021, **13**, e00850.
61 V. Sabna, S. G. Thampi and S. Chandrakaran, *Ecotoxicol. Environ. Saf.*, 2016, **134**, 390–397.
62 R. Saleh, A. H. Zaki, F. I. A. El-Ela, A. A. Farghali, M. Taha and R. Mahmoud, *J. Environ. Chem. Eng.*, 2020, 104726.
63 F. Bibi, A. Sattar, S. Hussain and M. Waseem, *Chem. Pap.*, 2023, **77**, 3957–3966.
64 D. Liang, Z. Ning, Z. Song, C. Wang, Y. Liu, X. Wan, S. Peng, Z. Liu and A. Lu, *Molecules*, 2019, **24**, 3453.
65 M. Bansal, N. Mittal, S. K. Yadav, G. Khan, P. Gupta, B. Mishra and G. Nath, *J. Oral Biol. Craniofac. Res.*, 2018, **8**, 126–133.
66 P. Zhang, *Ke Res. Gr.*, 2016, 1–19.
67 A. Kumar and H. M. Jena, *Results Phys.*, 2016, **6**, 651–658.
68 Y. Zhang, K. Liu, X. Liu, W. Ma, S. Li, J. Wang and S. Fan, *J. Mater. Sci. Mater. Electron.*, 2021, **32**, 18728–18740.
69 E. E. Jasper, V. O. Ajibola and J. C. Onwuka, *Appl. Water Sci.*, 2020, **10**, 1–11.
70 J. Rojas, D. Suarez, A. Moreno, J. Silva-Agredo and R. A. Torres-Palma, *Appl. Sci.*, 2019, **9**, 5337.
71 Y. Raji, A. Nadi, I. Mechnou, M. Saadouni, O. Cherkaoui and S. Zyade, *Diam. Relat. Mater.*, 2023, **135**, 109834.
72 R. Goswami and A. K. Dey, *Adsorpt. Sci. Technol.*, 2022, **2022**, 2357242.
73 R. Aydogmus, T. Depci, M. Sarikaya, A. R. Kul and Y. Onal, in *IOP Conference Series: Earth and Environmental Science*, IOP Publishing, 2016, vol. 44, p. 52022.
74 M. Goswami and P. Phukan, *J. Environ. Chem. Eng.*, 2017, **5**, 3508–3517.
75 F. Mustafanejad, N. Sajjadi, R. Marandi and M. Zaeimdar, *Nanotechnol. Environ. Eng.*, 2021, **6**, 30.
76 N. A. H. Alshammari, J. S. Alnawmasi, A. M. Alotaibi, O. A. O. Alshammari, M. A. Abomuti, N. H. Elsayed and A. A. El-Bindary, *Process Saf. Environ. Prot.*, 2024, **190**, 353–371.
77 W. Fritz and E.-U. Schluender, *Chem. Eng. Sci.*, 1974, **29**, 1279–1282.
78 O. Redlich and D. L. Peterson, *J. Phys. Chem.*, 1959, **63**, 1024.
79 R. Sips, *J. Chem. Phys.*, 1948, **16**, 490–495.
80 M. Goncalves dos Santos, L. Destefani Paquini, P. H. Leite Quintela, L. P. Roberto Profeti and D. Guimarães, *ACS Omega*, 2025, **10**, 20326–20340.

81 A. M. Alotaibi, J. S. Alnawmasi, N. A. H. Alshammari, M. A. Abomuti, N. H. Elsayed and M. G. El-Desouky, *Int. J. Biol. Macromol.*, 2024, **274**, 133442.
82 C. W. Rizkita, L. Qadariyah, M. Mahfud and S. Sukardi, *Egypt. J. Chem.*, 2025, **68**, 333–341.
83 E. P. Kuncoro, T. Soedarti, T. W. C. Putranto, H. Darmokoesoemo, N. R. Abadi and H. S. Kusuma, *Data Br.*, 2018, **16**, 908–913.
84 R. Baronia, J. Goel, J. Kaswan, A. Shukla, S. K. Singhal and S. P. Singh, *Mater. Renew. Sustain. Energy*, 2018, **7**, 1–13.
85 S. M. Mahgoub, M. R. Mahmoud, A. Y. Binsaleh, M. A. Almalki, M. A. Mohamed and H. F. Nassar, *Sustain. Chem. Pharm.*, 2023, **36**, 101291.
86 H. M. Nassef, H. A. Ahmed, A. H. Bashal, M. A. El-Atawy, T. Y. A. Alanazi, S. M. Mahgoub and M. A. Mohamed, *Rev. Anal. Chem.*, 2024, **43**, 20230073.
87 F. Pena-Pereira, W. Wojnowski and M. Tobiszewski, *Anal. Chem.*, 2020, **92**, 10076–10082.
88 A. Wathukarage, I. Herath, M. C. M. Iqbal and M. Vithanage, *Environ. Geochem. Health*, 2019, **41**, 1647–1661.
89 M. U. Dao, H. S. Le, H. Y. Hoang, V. A. Tran, V. D. Doan, T. T. N. Le, A. Sirotkin and V. T. Le, *Environ. Res.*, 2021, **198**, 110481.